



HAL
open science

Experimental study and modelling of the phase transformation of Zircaloy-4 alloy under high thermal transients

T. Jailin, Nicolas Tardif, J. Desquines, Michel Coret, M.-C. Baietto, V. Georghum

► To cite this version:

T. Jailin, Nicolas Tardif, J. Desquines, Michel Coret, M.-C. Baietto, et al.. Experimental study and modelling of the phase transformation of Zircaloy-4 alloy under high thermal transients. *Materials Characterization*, 2020, 162, pp.110199. 10.1016/j.matchar.2020.110199 . hal-02489746v2

HAL Id: hal-02489746

<https://hal.science/hal-02489746v2>

Submitted on 12 Jul 2022

HAL is a multi-disciplinary open access archive for the deposit and dissemination of scientific research documents, whether they are published or not. The documents may come from teaching and research institutions in France or abroad, or from public or private research centers.

L'archive ouverte pluridisciplinaire **HAL**, est destinée au dépôt et à la diffusion de documents scientifiques de niveau recherche, publiés ou non, émanant des établissements d'enseignement et de recherche français ou étrangers, des laboratoires publics ou privés.



Distributed under a Creative Commons Attribution - NonCommercial - NoDerivatives 4.0 International License

Experimental study and modelling of the phase transformation of Zircaloy-4 alloy under high thermal transients

T. Jailin^{a,b}, N. Tardif^{b,*}, J. Desquines^a, M. Coret^c, M.-C. Baidetto^b, V. Georghenthum^a

^aInstitut de Radioprotection et de Sûreté Nucléaire (IRSN), PSN-RES, Cadarache, Saint Paul lez Durance, France

^bUniv Lyon, INSA-Lyon, CNRS UMR5259, LaMCoS, F-69621, France

^cÉcole Centrale de Nantes, GeM (UMR 6183), Nantes, France

Abstract

Dilatometry tests were performed to study the phase transformation kinetic of nuclear fuel claddings made of Zircaloy-4 upon fast heating rates (up to 2000°C/s). These tests highlighted that from equilibrium to 500°C/s the temperature at which the transformation starts shifts towards higher temperatures with increasing heating rates. Above 500°C/s no impact of the heating rate was observed. The temperature at which the transformation ends remains close to 960°C with no clear dependence on heating rate. Metallurgical analyses were carried out and were in agreement with the results obtained by dilatometry. A phase transition model was identified from equilibrium to 2000°C/s.

Keywords: Fast thermal transients, Phase transformation, Dilatometry, Zircaloy-4

1. Introduction

The thermo-mechanical properties of materials are strongly related to their microstructure. Subsequently, the study of the allotropic phase transition has been of great interest for structural materials, especially the ones used at high temperatures [1, 2]. Many previous researchers have shown the impact of the thermal kinetic on the phase transition of materials. However, due to experimental difficulties, few studies were devoted to the analysis of the material phase transition under high heating rates, the great majority focusing on low heating rates or high cooling rates [3, 4]. This present work aims at introducing some new results about the phase transition of the Zircaloy-4 alloy upon very high heating rates.

Zircaloy-4 is widely used in Pressurized Water Reactor (PWR) as fuel cladding material. Improving the validity range of its thermo-mechanical behavior is an important challenge in the nuclear safety domain. This is especially true in accidental situations, where the loading conditions can be very intense. The Loss Of Coolant Accident (LOCA) and the Reactivity Initiated Accident (RIA) are the two design basis accidents studied for PWR. Heating rates below 100°C/s are expected on the claddings during a LOCA. It can exceed 1000°C/s during the post-Departure from Nucleate Boiling (DNB) phase of a RIA [5]. In both accidents the temperature of the cladding can reach upwards of 1000°C.

Zircaloy-4 presents an allotropic phase transformation ($\alpha \rightarrow \beta$) between 800°C and 1000°C upon heating at equilibrium. Its crystallographic structure transforms from a hexagonal closed packed structure, below 800°C, to a body centered cubic structure around 1000°C [6]. Between these two temperatures a two

phases mixture is present within the material. Since the metallurgical state of the material has a strong impact on its mechanical properties [7, 8, 9, 10, 11] many authors have devoted their studies to the impact of the thermal kinetic on the phase transition. Forgeron *et al.* [7], for instance, investigated the phase transformation of Zircaloy-4 and M5 alloy in equilibrium, heating and cooling conditions. They used calorimetry and dilatometry techniques to study the effect of the thermal transient for rates up to 100°C/s. Others methods have also been used, such as in-situ synchrotron X-ray diffraction (SXRD) or resistivity tests [12, 13].

The general literature agrees on the point that the phase transformation is delayed toward higher temperatures as the heating rate increases. However, the phase transition of Zircaloy-4 has not been investigated for heating rates above 100°C/s. This can be explained by the difficulty of reproducing experimentally well-controlled fast thermal transients. Accurate temperature measurement is difficult at very high heating rates. The extrapolation of the existing transition models [7, 14] to heating rates greater than 100°C/s is then not straightforward.

In this work, dilatometry tests were carried out on as-received Zircaloy-4 claddings with heating rates up to 2000°C/s. Special care was taken to the thermal and the kinematic measurements. The dilatometry conclusions were supported by micrographs. Finally, a phase transformation model based on the kinetic equation of Leblond [15] was identified, reproducing the measurements on Zircaloy-4 samples from equilibrium to 2000°C/s.

The first section deals with the experimental setup, the methods and the phase transition model. The experimental results and the identification of the model are presented in the second section. The third section discusses the important features that have to be taken into account to perform a dilatometry test at

*Corresponding author

Email address: auteur@insa-lyon.fr (N. Tardif)

high thermal slope. An updated model is also proposed to re-
 65 produce the phase transition under fast heating rates.

2. Experimental setup and methods

2.1. Specimen and device

Stress-free dilatometry experiments were performed using a
 GLEEBLE-3500 device [16]. Specimens were cut from Stress
 70 Relieved Annealed (SRA) Zircaloy-4 (Zr-4) claddings (see the
 chemical composition in Table 1). The microstructure of the
 as-received material is composed of thin and elongated grains
 and presents a texture having the $\langle c \rangle$ direction at $\pm 30^\circ$ from
 the radial direction of the tube [17]. The samples have an initial
 75 eccentricity of between 1 and 3% [18].

Sn	Fe	O	Cr	C	Zr
1.29	0.21	0.13	0.11	0.016	bal.

Table 1: Stress relieved annealed Zircaloy-4 composition (in wt%).

Specimens were 100mm long tubes, with an external diam-
 eter of 9.5mm and a wall-thickness of 0.57mm. Custom jaws
 enabled heating rates up to 2800°C/s to be reached by Joule
 heating, with perfect axisymmetric thermal distribution. A pic-
 80 ture of a sample mounted on the device is given in Figure 1.
 One side of the sample is fixed and the other one is free along
 its axial direction. The distance between the jaws is 40mm.

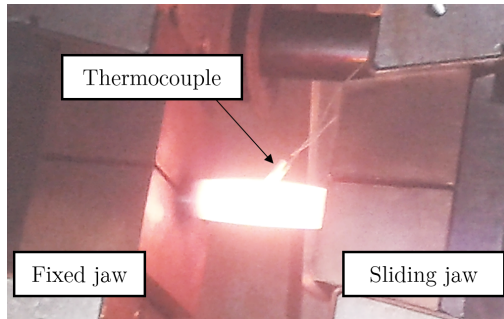


Figure 1: Picture of a sample mounted on the device.

In order to have a constant emissivity on the sample outer sur-
 face during the experiments, the specimens were pre-oxidized
 85 during two days in a furnace at 470°C under air environment.
 A uniform oxide layer of $2.5\mu\text{m}$ was thus obtained, keeping the
 material texture and the material state unchanged. 30mm were
 then sandblasted on each end of the tubular sample to have a
 good electric conduction with the jaws.

2.2. Tests processing

Two kinds of tests were performed to investigate the impact
 of the heating rate on the phase transformation. A first batch
 of specimens was used to study the phase transformation by
 dilatometry. The test procedure of these experiments is depic-
 95 tured in Figure 2. The sample was first heated at 400°C . After
 a 10 seconds plateau, the thermal transient was applied until

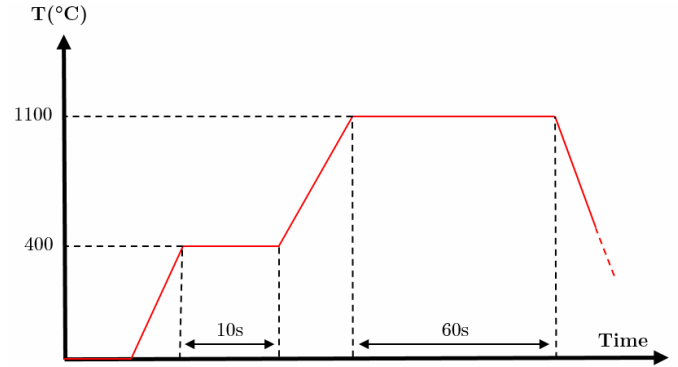


Figure 2: Temporal evolution of the thermal loading applied during the dilatometry tests.

1100°C . The temperature was then maintained 60 seconds be-
 fore cooling down by cutting off the power.

A second batch of specimens was used to perform metallur-
 gical analysis by optical microscopy. Similarly to the first tests
 the samples were first heated at 400°C . Then, after a 10 seconds
 hold, the thermal transient was applied until a "quenching" tem-
 perature T_q directly followed by a rapid cooling down by cutting
 off the power. A cooling rate of around -50°C/s was thus ob-
 tained. An example of a temperature record obtained is given
 in Figure 3 for a test carried out with a heating rate of 100°C/s ,
 until a quenching temperature of 910°C .

The two kinds of tests were performed under primary vac-
 uum (around 0.6mbar) to prevent the sample oxidation.

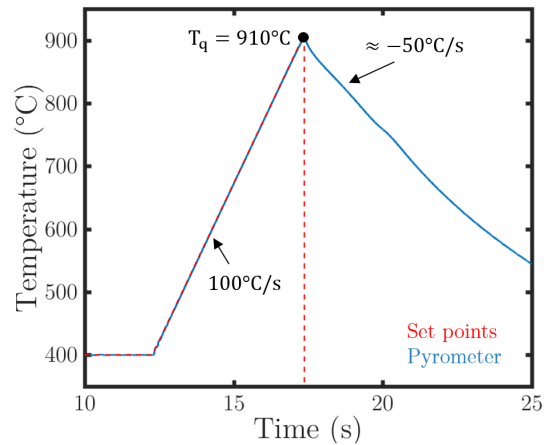


Figure 3: Example of a thermal response of a specimen from the second batch. This test was carried out with a heating rate of 100°C/s till a temperature $T_q = 910^\circ\text{C}$ (pyrometer measurements).

2.3. Thermal measurement

A scheme of the device and the means of measurements is
 given in Figure 4.

The temperature was controlled during the tests at the cen-
 ter of the sample using a Metis M322 pyrometer (wavelength
 of $\lambda = [1.45 - 1.65] \mu\text{m}$, spot size of 2.5 mm). Radiometric
 measurement is not intrusive but is very sensitive to the emis-
 sivity. The sample emissivity has to be known accurately and

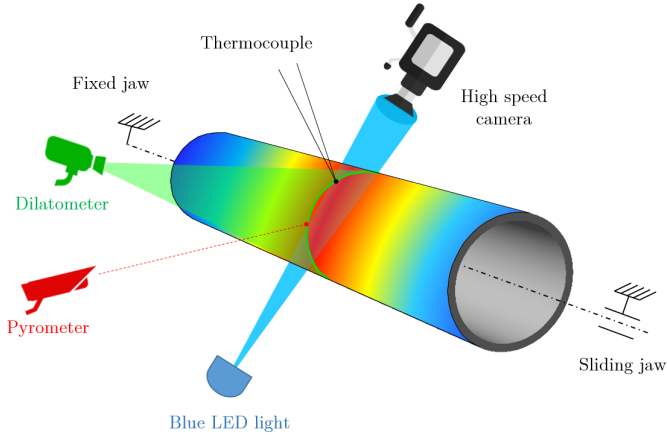


Figure 4: Scheme of the setup.

must remain constant during the tests. Even under secondary vacuum (around 10^{-3} mbar) a thin oxide layer develops on the sample surface at temperatures above 800°C . On as-received material this leads to a significant change of the emissivity that distorts the pyrometer measurements. It is then convenient to pre-oxidize the samples with a thin oxide layer so that additional oxidation no longer modifies the emissivity during the tests. The samples were hence pre-oxidized with a uniform oxidation layer that stabilizes the emissivity during the tests. The emissivity of the pre-oxidized samples was evaluated to be 0.955 ± 0.015 and remained unchanged during 20min at 1100°C . The pyrometer leads to an accuracy of around 0.7% of the temperature.

A type K thermocouple (diameter wires of 0.18mm) was spot-welded at the center of the specimen to obtain an additional thermal measurement during the temperature plateau and identify the emissivity of the sample. Due to a eutectic point between Nickel and Zirconium around 950°C , a thin square of Tantalum (thickness of 0.025mm) was inserted between the sample and the thermocouple.

The axial thermal profile on the sample was estimated by Near InfraRed Thermography (NIRT) [19, 20]. This full-field method links the digital level intensity I of an image (*i.e.* the gray level of each pixel) to the temperature T using a radiometric model based on Planck's law:

$$T = \frac{K_1}{\ln\left(\frac{K_2}{I} + 1\right)}. \quad (1)$$

In this model, two constants, K_1 and K_2 , are identified using the pyrometer data during the thermal transient. Using a high speed camera Phantom V710 at 2000Hz, an axial thermal profile was characterized on the specimens during the transient and the plateau.

2.4. Thermal expansion measurements

The diametrical expansion was measured at the mid section of the specimen by contour detection method [21]. One high speed camera Phantom V710 1MPx ($1 \text{ px} \simeq 23\mu\text{m}$) recorded

pictures during the tests and a 200mm macro optic (NIK AF MICRO-NIKKOR 200MM F/4 D IF-ED) was mounted on the camera. The software UFreckles [22] was used to perform the images analysis. In order to avoid problems of radiation at high temperatures the sample was lighted using a blue LED ring (wavelength of $\lambda = 470\text{nm}$), and a pass band filter of the same wavelength was mounted on the optic [23] (*cf.* scheme of the setup in Figure 4). The dilatometry measurements are performed in a 3mm long portion of the tube, as presented in Figure 5. This method allows a subpixel precision and leads to an accuracy on the thermal expansion less than $1\mu\text{m}$.

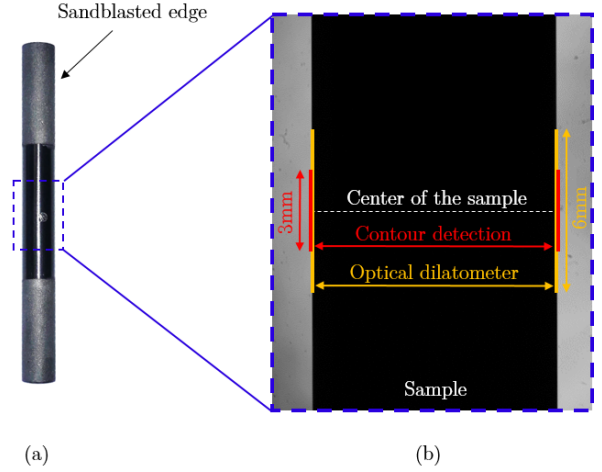


Figure 5: (a) Picture of a sample; (b) example of an image obtained with the high speed camera. The diametrical expansion is computed between the red lines by contour detection method and between the orange lines with the optical dilatometer.

An optical dilatometer (KEYENCE LS-7600) was also used to obtain an additional measurement of the diametrical expansion with an accuracy of around $5\mu\text{m}$. The length of the measurements area of the dilatometer is around 6mm. Maximal frequencies of 2000Hz and 7500Hz could be obtained for the dilatometer and the high speed camera, respectively. Both means of measurements led to comparable results but the contour detection method led to less noisy data. Therefore, contour detection measurements were used to compute the phase fractions.

2.5. Phase fraction computation

The lever rule is usually used to compute the phase fraction from the dilatometry curves. The principle of the method is described in Figure 6. In order to get proper results the dilatometry curves are first smoothed using a Gaussian filter. The authors point out that due to its nature, the lever rule method does not enable an accurate estimation of the phase content in the boundaries of the dual phase domain (*i.e.* from 0 to 10% and from 90 to 100% of β phase).

2.6. Kinetic model

The kinetic model of Leblond [15] is used to model the ($\alpha \rightarrow \beta$) phase transformation. This model enables reproducing anisothermal transformations, including diffusion con-

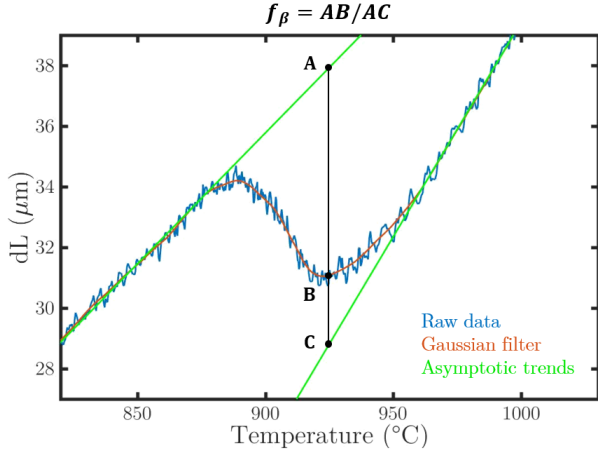


Figure 6: Scheme of principle of the lever rule method. The phase fraction of β is computed such as $f_{\beta} = AB/AC$.

trolled transformations and martensitic transformations. The Leblond's evolution equation is given by:

$$\frac{df_{\beta}}{dt} = \frac{f_{eq}(T) - f_{\beta}}{\tau(T)}, \quad (2)$$

where $f_{eq}(T)$ is the fraction of β at equilibrium at the temperature T and $\tau(T)$ represents the characteristic time of transformation, *i.e.* at a temperature T , f_{β} tends towards $f_{eq}(T)$ in a time equal to $\tau(T)$.

It is usual and convenient to describe $\tau(T)$ by an Arrhenius-type equation such as:

$$\tau(T) = \left[k_0 \cdot e^{-\frac{E}{RT}} \right]^{-1}, \quad (3)$$

where k_0 is a kinetic prefactor, E is an activation energy and R is the perfect gas constant. Two constants, k_0 and E , have finally to be identified. It is chosen to represent the equilibrium function f_{eq} with the equation of Forgeron [7] that is:

$$f_{eq}(T) = 1 - e^{-[C \cdot (T - T_0)]^n}, \quad (4)$$

where $C = 1/(T_{63.2\%} - T_0)$, $T_{63.2\%}$ is the temperature corresponding to 63.2% of β phase at equilibrium, T_0 is the temperature at the beginning of the transformation at equilibrium and n is an exponent to adjust. For Zircaloy-4: $C = 1.135 \cdot 10^{-2} \text{ } ^\circ\text{C}^{-1}$, $T_0 = 809^\circ\text{C}$ and $n = 2.187$.

The parameters of the model (Equation 2) are identified using the dilatometry measurements by minimizing the cost function defined such as:

$$er^2(\lambda) = [U_{exp} - U_{num}(\lambda)]^2, \quad (5)$$

where λ is the set of parameters to identify, U_{exp} are the raw experimental values of thermal expansion and U_{num} are the numerical values of thermal expansion. U_{num} is computed as:

$$U_{num} = U_{\alpha}(T) \cdot (1 - f_{\beta}) + U_{\beta}(T) \cdot f_{\beta}, \quad (6)$$

where U_{α} and U_{β} are the asymptotic linear trends of the measured displacement in the α and β domain, respectively.

3. Experimental results

3.1. Dilatometry results

Around 20 dilatometry tests were performed following the procedure described in Figure 2. The heating rates imposed varied from 50 to 2000 $^\circ\text{C/s}$ (see Table 2).

Exp. no.	dT/dt ($^\circ\text{C/s}$)	CTE α ($10^{-6} \text{ } ^\circ\text{C}^{-1}$)	CTE β ($10^{-6} \text{ } ^\circ\text{C}^{-1}$)
D1	50	12	13
D2	50	9.7	13
D3	75	8.5	12
D4	75	9.5	13
D5	100	8.7	14
D6	100	9.2	16
D7	150	8.8	17
D8	200	9.6	14
D9	200	10	13
D10	350	10	15
D11	500	8.0	12
D12	600	10	12
D13	600	9.6	12
D14	800	9.3	12
D15	1000	8.2	13
D16	1000	9.5	12
D17	1200	9.9	11
D18	1400	11	12
D19	1400	9.9	15
D20	2000	9.7	13

Table 2: Dilatometry tests performed with the associated values of heating rates, and coefficients of thermal expansion (CTE).

For the experiments carried out with imposed heating rates greater than 100 $^\circ\text{C/s}$, a decrease of the heating rate was observed during the phase transformation. Figure 7.a shows the thermal response recorded by the pyrometer for a test performed with a heating rate imposed at 2000 $^\circ\text{C/s}$. It is observed that the heating rate decreases during the phase transition, till a minimal value of 780 $^\circ\text{C/s}$. The evolution of the heating rate obtained for different specified heating rates are given in Figure 7.b. It is observed that the heating rate decreases from around 870 to 950 $^\circ\text{C}$, *i.e.* the range of the phase transition.

Figure 8 depicts examples of dilatometry curves obtained. Equation 4 models the equilibrium function f_{eq} .

The phase transition domain is characterized in Figure 8 by the loss of linearity in the coefficient of thermal expansion (CTE).

3.2. Identification of the model

The equilibrium (Figure 8) and the tests performed with a heating rate ranging from 50 to 500 $^\circ\text{C/s}$ are used to identify the model described in section 2.6. The equilibrium parameters

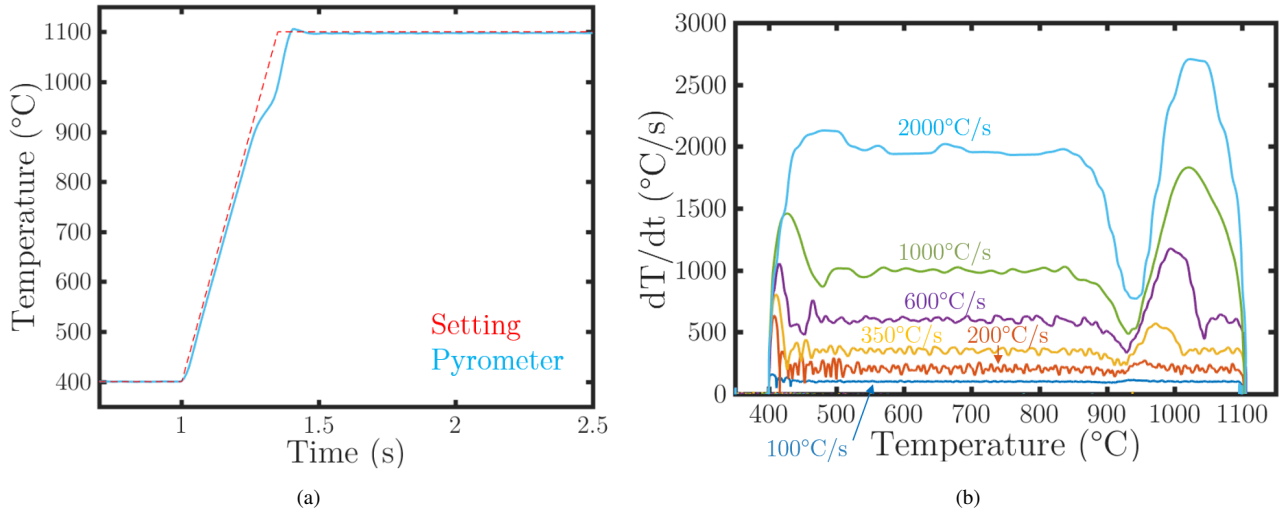


Figure 7: (a) Pyrometer measurements for a test carried out with a heating rate imposed at 2000°C/s. (b) Evolution of the heating rate for several specified values. The values on the right correspond to the heating rates imposed during the tests.

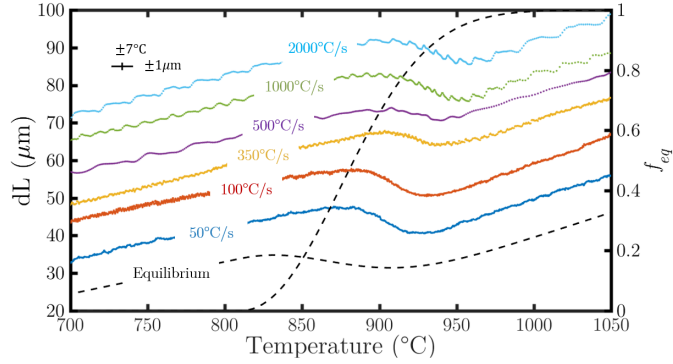


Figure 8: Examples of dilatometry curves. The equilibrium curves were obtained using the Equation 4. An offset along the y axis is added on the dilatometry curves for a better readability.

(C , T_0 and n) are re-identified to allow some flexibility to the identification algorithm and to take into account uncertainties. Finally, five parameters are identified: C , T_0 and n of Equation 4 and k_0 and E of Equation 3. The final values are given in Table 3.

C ($^{\circ}\text{C}^{-1}$)	T_0 ($^{\circ}\text{C}$)	n	$\ln(k_0)$	E ($\text{kJ}\cdot\text{mol}^{-1}$)
$6.89 \cdot 10^{-3}$	750	4.14	79.62	764.2

Table 3: Identified parameters of Equations 3 and 4.

Figure 9 compares some dilatometry curves obtained experimentally to the ones obtained with the model. The fraction of β obtained for different heating rates with the model is given in Figure 10.a. The authors remind that the β fraction is not reliable between 0 and 10% and between 90 and 100%. It can be observed that for all the tests the end of transformation occurs around 960°C. It is in good agreement with the results of [10]. On the other hand the temperature at which the transformation starts increases with the heating rate. The equilibrium curve re-

identified matches well on the equilibrium curve of Forgeron. The difference in the β fraction remains below 5%.

The Figure 10.b shows the evolution of the temperature $T_{50\%}$, at which the phase fraction of β is equal to 50%, obtained by the model versus the heating rate. From equilibrium to 500°C/s $T_{50\%}$ phase increases from 880 to 933°C. It stabilizes at higher heating rates.

3.3. Metallurgical analysis

The as-received microstructure of the samples is presented in Figure 11. The material is composed of thin and elongated grains as usually found in the literature [17].

Metallurgical analysis were performed after three different heating transients of 50, 100 and 1200°C/s. These experiments followed the procedure describes in Figure 3. Examples of optical micrographs are given in Figure 12.

After quenching at 910°C the microstructure strongly differs from the one of the as-received material. For the three heating rates, grains are small and equiaxed. It can be deduced that recrystallization occurred. It is in good agreement with the recrystallization kinetics expected from [24, 25]. Some micro α needles are precipitated within the grains for the experiment performed at 50°C/s. Fewer α needles are observed for the experiment performed at 100°C/s. No ones are observed for the test performed at 1200°C/s. These micro α needles are characteristic of ex- β grains at high temperature. Though a quantitative estimation of the phase fraction is not possible with these micrographs, a qualitative comparison can be done. No, or few β grains were present for the experiments performed at 1200°C/s. Some β grains must have been formed in the material for the experiments performed at 50 and 100°C/s.

At 950°C the grains still have the same morphology. However many micro α needles appear within many grains. It is characteristic of a high β phase content within the material at this temperature.

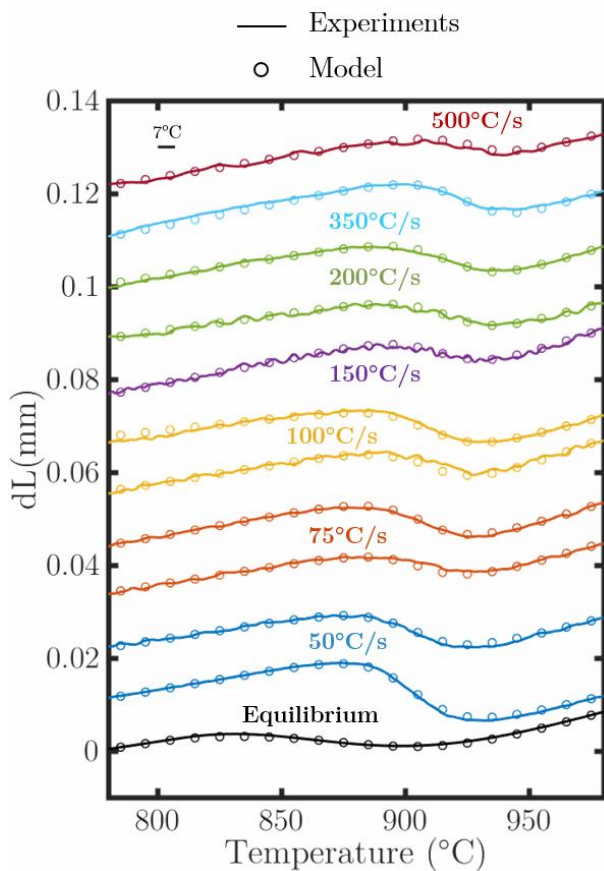


Figure 9: Examples of dilatometry curves obtained (full lines) and results of the model (circle marks). An offset along the y axis is added on the dilatometry curves for a better readability.

Above 980°C, the grains size significantly increases and macro needles are visible. This steep evolution in the microstructure can be explained by the full dissolution of small α inclusions existing at slightly lower temperature at the ex- β grains boundaries. This few remaining α phase would prevent the growth of the β grains by anchoring the grain boundaries. After full transformation into β phase would then release the β grains growth and lead to the microstructure observed in Figure 12. The grain size continues to increase with the temperature as shown in Figure 12.d for a sample quenched at 1001°C.

Similar conclusions were obtained by some authors. Trego [26] evidenced a fast increase of the β grains size at the $(\alpha + \beta) \rightarrow \beta$ transition for the M5 alloy. Romero [27] highlighted also this phenomenon for the Zircaloy-2 alloy at low heating rates.

These micrographs are in good agreement with the dilatometry curves of Figure 8. In the vicinity of 960°C the $(\alpha \rightarrow \beta)$ transformation seems complete, and at 950°C a high proportion of β phase is expected. The comparison between the micrographs of the samples quenched at 910°C are also consistent with dilatometry results. These observations are also corroborated by the creep tests and the micrographs performed in [10] on Zircaloy-4 samples. A steep transition in the creep rate and a fast increase of the grain size was evidenced in the vicinity of 970°C.

4. Analysis and discussions

If one wants to perform dilatometry tests with fast heating transients (*i.e.* > 50°C/s), two important aspects have to be taken into account in the test setup : the measurement of the temperature and the thermal heterogeneity on the thermal expansion measurement area.

4.1. The measurement of the temperature

The use of thermocouples to measure the temperature during thermal transients may be inadequate. Systematic error has to be taken into account due to the intrusive nature of this measurement technique, especially for fast thermal transients. This systematic error is favored by high heating rates and large thermocouples wire diameter. Figure 13 shows a comparison between the pyrometer and a thermocouple measurements, for a test carried out with a heating rate of 100°C/s till 1100°C. It is observed that the values given by the thermocouple are around 25°C lower than the pyrometer ones during the transient. The use of radiometric measurements becomes then necessary to avoid such errors. **The inertia effect of the thermocouple can be estimated at the first order by finite element calculations as presented in Appendix A.**

It is also worthy to analyse the values of CTE obtained at different heating rates. The CTE should not be dependent of the heating rate without activation of metallurgical phenomenon (*i.g.* phase transformation or elements dissolution) in the material. Such a dependence is observed when using thermocouples to measure fast thermal transients.

For the tests supporting the present study, the CTE in the α domain is found to be equal to $9.6 \cdot 10^{-6} \pm 0.9 \cdot 10^{-6} \text{ } ^\circ\text{C}^{-1}$ and

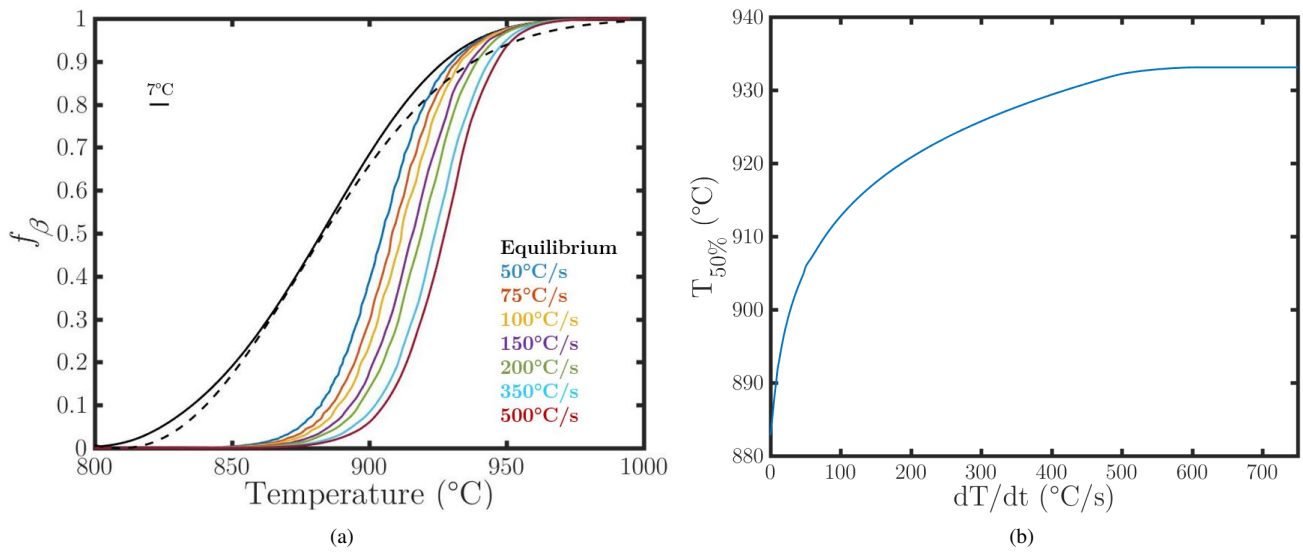


Figure 10: (a) Fraction of β obtained. The black dashed curve corresponds to the equilibrium of [7], the full lines correspond to the model computed with the true experimental thermal data. The heating rates correspond to the set points. (b) Evolution of the temperature at which the phase fraction of β is equal to 50% as a function of the heating rate (results of the model).

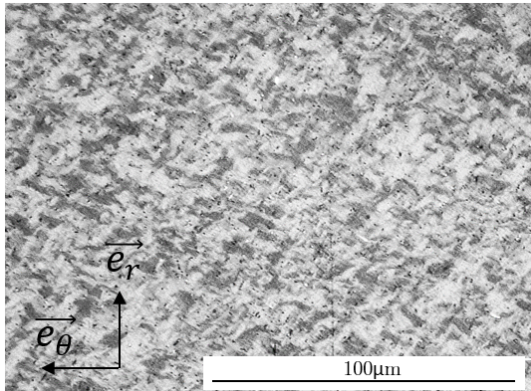


Figure 11: Optical micrograph of the as-received material (polarized light, radial cut).

the CTE in the β domain is found to be equal to $1.32 \cdot 10^{-5} \pm 1.5 \cdot 10^{-6} \text{ } ^{\circ}\text{C}^{-1}$ (cf. Table 2). These values were found relying on the pyrometer temperature measurements. No impact of the thermal slope was observed on the CTE.

4.2. Homogeneous temperature area

The thermal measurements can usually be considered as local, if a thermocouple or a pyrometer are used. Conversely, the thermal expansion measurements are usually performed over a more or less important area (cf. Figure 5). As a consequence, the thermal expansion recorded corresponds to the average value within this area. It is then important to notice that a thermal heterogeneity in the sample may lead to significant errors in the phase fraction computation. This is because the phase transition may not occur simultaneously throughout the area where the thermal expansion measurements are performed.

It follows that the phase fraction obtained cannot be linked to the temperature measured locally.

To study the impact of a heterogeneous temperature in the thermal expansion measurements area a bar of Zircaloy-4 having a length L is numerically simulated. The CTE of the α and β phases are set equal to $9.6 \cdot 10^{-6} \text{ } ^{\circ}\text{C}^{-1}$ and $1.33 \cdot 10^{-5} \text{ } ^{\circ}\text{C}^{-1}$, respectively. Forgeron's model (Equation 4) is used to simulate the phase transition. The bar is heated from room temperature to 1200 $^{\circ}\text{C}$ with a parabolic axial thermal distribution. Five levels of heterogeneity are simulated. The phase fraction is then recomputed in the whole area using the lever rule method. The results are presented in Figure 14. For thermal heterogeneity of $\{5, 10, 20, 50, 100\}^{\circ}\text{C}$ the maximal differences in the phase fraction measured with the reference are around $\{1.5, 3, 7, 18, 32\}\%$, respectively. The estimation of the thermal heterogeneity in the thermal expansion measurements area, by full-field method for instance, is then necessary to avoid an averaging effect.

The thermal distribution on the samples in the dilatometry tests was estimated using the NIRT method. Figure 15 shows an example of an image obtained with the associated thermal profile. A homogeneous temperature area of about 7mm was observed at the center of the sample, with an acceptable thermal heterogeneity of 5 $^{\circ}\text{C}$. The temperature and the diametrical expansion were measured in this area.

The temperature variation through the section was estimated to be lower than 4 $^{\circ}\text{C}$ by finite element calculations (cf. Appendix A). It has then a small impact on the phase fraction computation ($< 1.5\%$).

4.3. Impact of the mechanical deformations

Finite element calculations were performed to study the impact of the mechanical deformation on the phase fraction com-

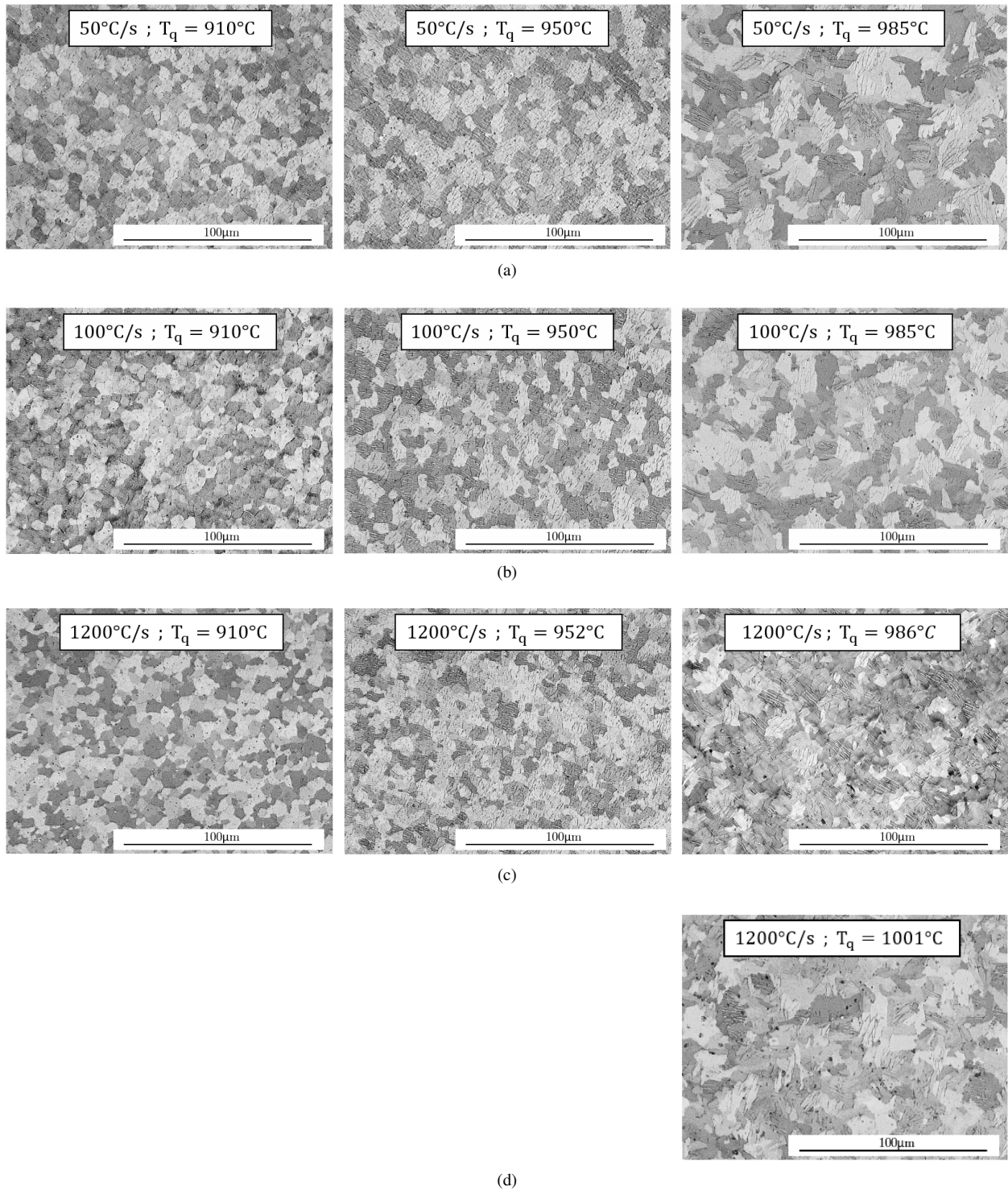


Figure 12: Optical micrographs for the experiments performed at: (a) 50°C/s, (b) 100°C/s, (c-e) 1200°C/s (polarized light, radial cut).

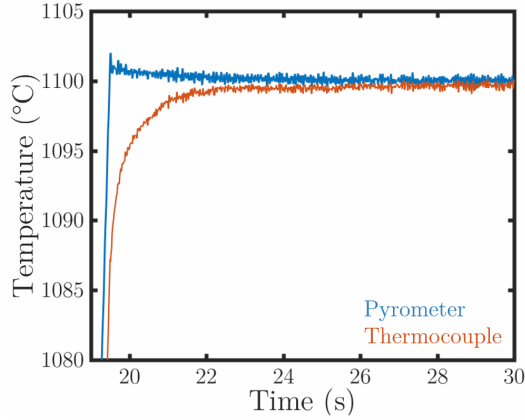


Figure 13: Comparison between the pyrometer and a thermocouple (type K, Wires diameter of 0.18mm) at 100°C/s.

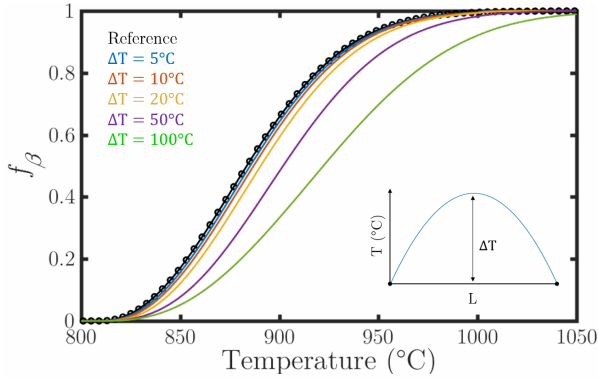


Figure 14: Impact of a quadratic thermal heterogeneity on the thermal expansion measurements. 5 values of thermal heterogeneity are presented for a bar of length L .

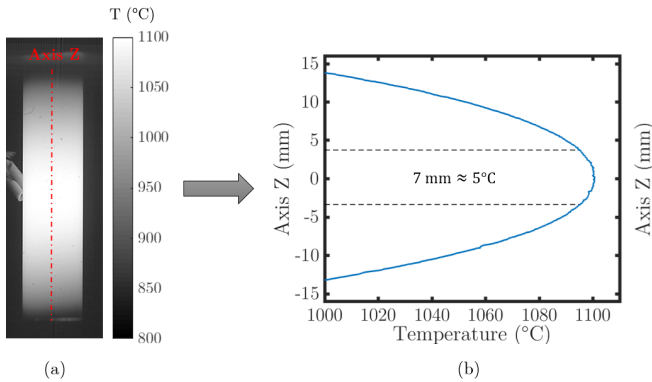


Figure 15: Results obtained by NIRT (a) Example of an image obtained with the high speed camera (temperature computed by NIRT); (b) Axial thermal profile extracted from the red line.

385 computation. More details of the modelling are given in Appendix A. The calculations show that the mechanical deformation is negligible compared to the total deformation and do not affect the phase fraction computed by the lever rule method.

4.4. Taking into account the saturation effect

390 The impact of the heating rate on the phase transformation kinetics appears to saturate above 500°C/s, at least within the uncertainties range of our means of measurement. Figure 16 shows the phase fraction obtained for the tests performed with heating rates varying from 500 to 2000°C/s. These curves were computed using the lever rule method described in section 2.5.

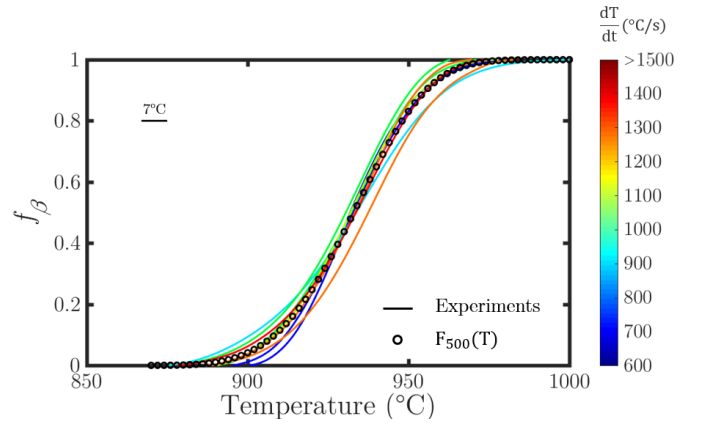


Figure 16: The full lines represents the evolution of f_β for the experiments carried out with heating rates above 500°C/s (Exp. no. D12 to D20 in Table 2). The circle marks represent the function $F_{500}(T)$.

395 To take into account this saturation effect a function F_{500} was defined to model the phase transformation kinetics for heating rate above 500°C/s. The same shape of Equation 4 was used so that:

$$F_{500}(T) = 1 - e^{-[C_2 \cdot (T - T_2)]^{n_2}}, \quad (7)$$

400 where C_2 , T_2 and n_2 can be linked to C , T_0 and n . The identified function F_{500} is depicted with the circle marks in Figure 16 and the three associated parameters are given in Table 4.

C_2 ($^{\circ}\text{C}^{-1}$)	T_2 ($^{\circ}\text{C}$)	n_2
$1.36 \cdot 10^{-2}$	865.4	4.18

Table 4: Parameters of the function $F_{500}(T)$.

The Equation 2 can now be updated such as:

$$\frac{df_\beta}{dt} = \begin{cases} \frac{f_{eq}(T) - f_\beta}{\tau(T)} & \text{if } f_\beta > F_{500}(T) \\ \frac{F_{500}(T) - f_\beta}{dt} & \text{otherwise.} \end{cases} \quad (8)$$

5. Summary and conclusions

The phase transition of Zircaloy-4 cladding was evaluated during fast thermal transients. Around 20 dilatometry tests were performed with heating rates ranging from 50 to 2000°C/s. It is shown that special care must be taken to the thermal measurements and the thermal homogeneity in the thermal expansion measurements area. A careful use of thermocouples is recommended during "fast" thermal transients. The thermal heterogeneity must also be accurately determined in the thermal expansion measurements area to avoid an averaging effect that may distort the dilatometry curves.

The tests evidenced several facts: (i) from equilibrium to 500°C/s the temperature at which the transformation starts shifts towards the high temperatures with increasing heating rates, (ii) above 500°C/s the heating rate effect saturates, (iii) the temperature at which the transformation ends (around 960°C) does not seem to be impacted by the heating rate.

A kinetic model based on Leblond's equation was identified. A function of saturation was added and the equilibrium equation was re-identified using the equilibrium data of [7]. This model is able to reproduce the phase transition of Zircaloy-4 claddings from equilibrium to heating rate till 2000°C/s and probably above considering the observed saturation of kinetic aspects. Further analysis will have to be conducted in order to use this model under cooling.

Experiments were carried out to perform metallurgical analysis. The micrographs confirmed that the transition in the pure β domain is expected at a temperature that is not significantly affected by the heating rate of about 960°C. The optical micrographs showed also a high fraction of β phase at 950°C for experiments performed at 50, 100 and 1200°C/s. It is in good agreement with the phase fraction found in the dilatometry experiments. Furthermore, all the results of this study are in good agreement with the creep results of [10] performed in post-DNB conditions.

It is worth noting that the phase transformation kinetic is influenced by the metallurgical state of the material. Nguyen [12] for instance, observed significantly faster phase transformation on recrystallized Zircaloy-4 than the same alloy in a stress relieved annealed metallurgical state. Additional testing is required to quantify the influence of the different parameters that may be coupled to the phase transformation (residual stress, lattice defects, initial microstructure...).

Data availability

The raw and processed data of the current study are available from the corresponding author on request.

Acknowledgments

The authors acknowledge with thanks financial support of this work from EdF and Institut Carnot Ingénierie@Lyon.

Appendix A. Finite element modelling of the experiments

Two modellings are performed to simulate the dilatometry experiments. A coupled thermal-electrical calculation is carried out to estimate the temperature variation through the cladding thickness and the inertia effect of the thermocouple. A thermo-mechanical calculation is performed to assess the impact of the mechanical deformations on the phase fraction computation. Both modellings are carried out using the Abaqus commercial software.

A.1. Coupled thermal-electrical calculation

The sample and the thermocouple are modelled using 8-node linear brick elements "DC3D8E". The cladding is modelled with an eccentricity of 3% [18] as schematized in Figure 17.a. The model is composed of 61626 elements and 6 elements are used through the cladding thickness. All the degrees of freedom are prescribed at one extremity of the sample and the other one has unconstrained displacements along the axial direction. The sample is heated by Joule heating from 20°C to 1100°C. Several heating rates are tested from 1 to 2000°C/s. The internal and external radiation is modelled. The convection is neglected, assuming that the experiments take place under vacuum. The material properties used to model the sample and the thermocouple are given in Table 5. These values are set to represent at the first order Zircaloy-4 and Chromel for the sample and the thermocouple, respectively. Figure 18 presents the finite element modelling.

Property	Sample	TC
Specific heat ($\text{J.kg}^{-1}.\text{K}^{-1}$)	375	600
Thermal conductivity ($\text{W.m}^{-1}.\text{K}^{-1}$)	25	19
Electrical resistivity ($\mu\Omega.\text{cm}$)	130	70.7
Density	6,6	8,7
Emissivity	0,9	0,9
Young's Modulus (GPa)	Eq. (9)	186

Table 5: Material properties used to model the sample and the thermocouple (TC).

$$E = 116.1 - 59 \times 10^{-3} \cdot T(K) \text{ [GPa]}. \quad (9)$$

Figure 17.b shows the circumferential thermal distribution obtained for a heating rate of 100°C/s. The temperature variation within the section is around 4°C. It has then an acceptable impact on the phase fraction computation, lower than 1.5% (cf. Figure 14).

Furthermore, the calculation enables obtaining a first order estimation of the inertia effect of the thermocouple. At 1000°C and for a heating rate of 100°C/s, the temperature in the vicinity of the thermocouple is 20°C lower than the temperature obtained at the opposite side of the tube. The authors point out that the inertia effect would be more important with a more realistic representation of the welding point.

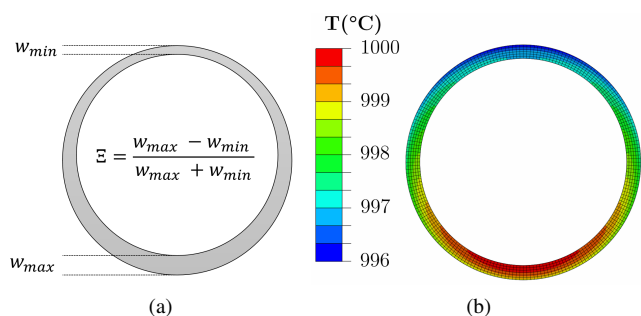


Figure 17: (a) Scheme to visualize the eccentricity Ξ imposed. w_{min} and w_{max} correspond to the minimal and maximal values of wall-thickness, respectively. (b) Temperature distribution obtained through the cladding section for a heating rate of 100°C/s and a sample eccentricity of 3%.

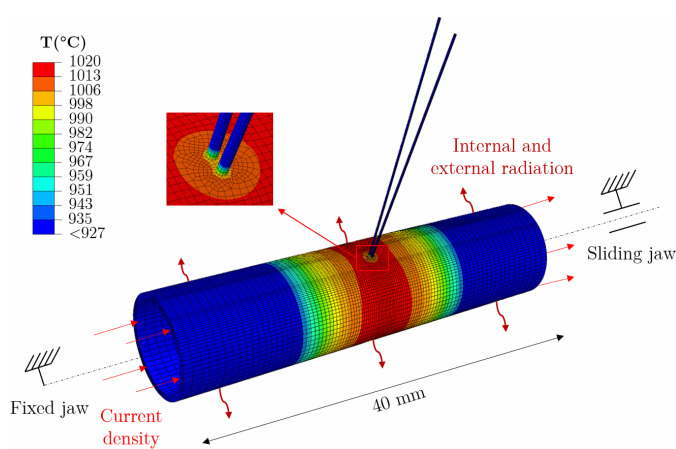


Figure 18: Results obtained for the thermal-electrical simulation for a heating rate of 100°C/s .

490 A.2. Thermo-mechanical calculation

An axisymmetric calculation is also performed to estimate the impact of the mechanical deformations on the phase fraction computation. The model is composed of 7020 elements "CAX4R" and 10 elements are used through the cladding thickness. The coefficient of thermal expansion of the material is set using the mean value of thermal expansion obtained during the dilatometry experiments. The phase transformation is simulated using the Equation (8). Thereby, the contraction obtained during the phase transformation is modelled. The sample is heated at different heating rates using the experimental temperature profiles measured by Near InfraRed Thermography (cf. Figure 15.b). A temperature variation of 4°C is imposed through the thickness. The jaws are cooled during the experience so the temperature at the extremities of the sample was set at 20°C . The Figure 19.a shows the axisymmetric model and the Figure 19.b shows the axial thermal profile imposed to the cladding at the end of the test.

The phase fraction is computed at the end of the calculation using the lever rule method at the middle of the sample in an area 5 mm long. A difference lower than 1.5% is obtained compared to the true phase content present at the middle of the sample.

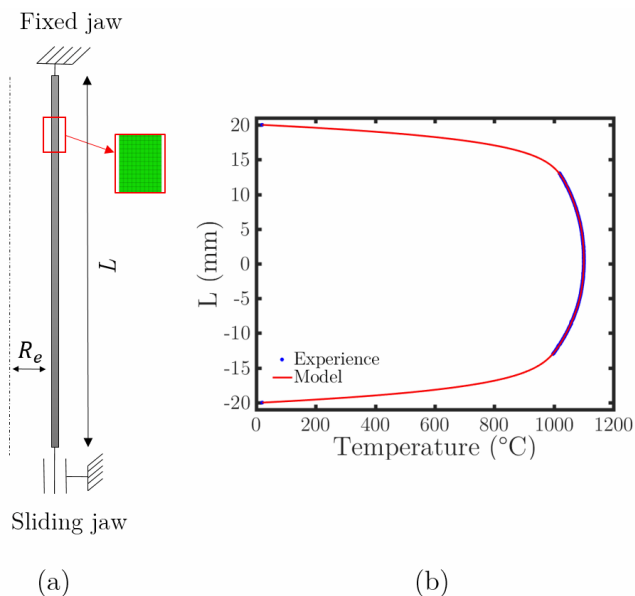


Figure 19: Thermo-mechanical modelling: (a) axisymmetric model; (c) axial thermal profile imposed to the cladding at the end of the test. The experimental points are obtained by NIRT and a polynomial function is used to fit the experimental points.

References

- [1] C. García De Andrés, F. G. Caballero, C. Capdevila, L. F. Álvarez, Application of dilatometric analysis to the study of solid-solid phase transformations in steels, *Materials Characterization* 48 (1) (2002) 101–111. doi:10.1016/S1044-5803(02)00259-0.
- [2] J. W. Elmer, T. A. Palmer, S. S. Babu, W. Zhang, T. DebRoy, Phase transformation dynamics during welding of Ti-6Al-4V, *Journal of Applied Physics* 95 (12) (2004) 8327–8339. doi:10.1063/1.1737476.
- [3] T. Ahmed, H. J. Rack, Phase transformations during cooling in alpha + beta titanium alloys, *Materials Science and Engineering: A* 243 (1-2) (1998) 206–211. doi:10.1016/S0921-5093(97)00802-2.
- [4] K. Nurveren, A. Akdo, Evolution of transformation characteristics with heating / cooling rate in NiTi shape memory alloys, *Journal of materials processing technology* 196 (1-3) (2007) 129–134. doi:10.1016/j.jmatprotec.2007.05.015.
- [5] V. Besson, Modelling of clad-to-coolant heat transfer for RIA applications, *Journal of Nuclear Science and Technology* 44 (2) (2007) 211–221. doi:10.1080/18811248.2007.9711275.
- [6] S. Banerjee, P. Mukhopadhyay, *Phase Transformations: Examples from Titanium and Zirconium Alloys*, Elsevier, 2010.
- [7] T. Forgeron, J. C. Brachet, F. Barcelo, A. Castaing, J. Hivroz, J. P. Mardon, C. Bernaudat, Experiment and Modeling of Advanced Fuel Rod Cladding Behavior Under LOCA Conditions: Alpha-Beta Phase Transformation Kinetics and EDGAR Methodology, in: *Zirconium in the Nuclear Industry: Twelfth International Symposium, 2000*, pp. 256–278. doi:10.1520/STP14303S.
- [8] R. A. Holt, The beta to alpha phase transformation in Zircaloy-4, *Journal of Nuclear Materials* 35 (1970) 322–334. doi:10.1016/0022-3115(70)90216-3.
- [9] E. J. Mittemeijer, Analysis of the kinetics of phase transformations, *Journal of Materials Science* 27 (15) (1992) 3977–3987. doi:10.1007/BF01105093.
- [10] T. Jailin, N. Tardif, J. Desquines, P. Chaudet, M. Coret, M.-C. Baietto, Thermo-mechanical behavior of Zircaloy-4 claddings under simulated post-DNB conditions, *Journal of Nuclear Materials* 531. doi:10.1016/j.jnucmat.2020.151984.
- [11] T. Jailin, N. Tardif, J. Desquines, M. Coret, M. C. Baietto, T. Bréville, P. Chaudet, V. Georgenthum, *Mechanical Behavior of As-Fabricated Zircaloy-4 Claddings Under the Simulated Thermo-Mechanical Post-*

- DNB Conditions of a Reactivity Initiated Accident (RIA), in: Top Fuel, European Nuclear Society, Prague, 2018.
- [12] C.-t. Nguyen, Microstructure Changes during Fast β Cycles of Zirconium Alloys, Ph.D. thesis, University of Manchester (2017).
- [13] D. Kaddour, S. Frechin, A. F. Gourgues, J. C. Brachet, L. Portier, A. Pineau, Experimental determination of creep properties of zirconium alloys together with phase transformation, *Scripta Materialia* 51 (6) (2004) 515–519. doi:10.1016/j.scriptamat.2004.05.046.
- [14] A. R. Massih, Transformation kinetics of zirconium alloys under non-isothermal conditions, *Journal of Nuclear Materials* 384 (3) (2009) 330–335. arXiv:0905.2276, doi:10.1016/j.jnucmat.2008.11.033. URL <http://dx.doi.org/10.1016/j.jnucmat.2008.11.033>
- [15] J.-B. Leblond, J. Devaux, A new kinetic model for anisothermal metallurgical transformations in steels including effect of austenite grain size, *Acta Metallurgica* 32 (I) (1984) 137–146. doi:10.1016/0001-6160(84)90211-6.
- [16] A. Mondelin, F. Valiorgue, M. Coret, E. Feulvarch, J. Rech, Procedia Engineering Surface integrity prediction in finish turning of 15-SPH stainless steel, *Procedia Engineering* 19 (2011) 270–275. doi:10.1016/j.proeng.2011.11.111. URL <http://dx.doi.org/10.1016/j.proeng.2011.11.111>
- [17] F. Li, T. Mihara, Y. Udagawa, M. Amaya, The effect of hydride morphology on the failure strain of stress-relieved Zircaloy-4 cladding with an outer surface pre-crack under biaxial stress states, *Journal of Nuclear Science and Technology* 56 (5) (2019) 432–439. doi:10.1080/00223131.2019.1592723.
- [18] D. Campello, N. Tardif, M. Moula, M. C. Baietto, M. Coret, J. Desquines, Identification of the steady-state creep behavior of Zircaloy-4 claddings under simulated Loss-Of-Coolant Accident conditions based on a coupled experimental/numerical approach, *International Journal of Solids and Structures* 115-116 (2017) 190–199. doi:10.1016/j.ijsolstr.2017.03.016.
- [19] Y. Rotrou, T. Sentenac, Y. Le Maoult, P. Magnan, J. Farré, Near infrared thermography with silicon FPA - Comparison to MWIR and LWIR thermography, *Quantitative InfraRed Thermography Journal* 3 (1) (2006) 93–115. doi:10.3166/qirt.3.93-115.
- [20] D. Campello, N. Tardif, J. Desquines, M. C. Baietto, M. Coret, A. Maynadier, P. Chaudet, Validation of a multimodal set-up for the study of zirconium alloys claddings' behaviour under simulated LOCA conditions, *Strain* 54 (5) (2018) 1–14. doi:10.1111/str.12279.
- [21] J. Réthoré, M. François, Curve and boundaries measurement using B-splines and virtual images, *Optics and Lasers in Engineering* 52 (2014) 145–155. doi:10.1016/j.optlaseng.2013.06.018.
- [22] J. Réthoré, *UFreckles v2* (2018). doi:10.5281/zenodo.1433776.
- [23] B. M. Grant, H. J. Stone, P. J. Withers, M. Preuss, High-temperature strain field measurement using digital image correlation, *Journal of Strain Analysis for Engineering Design* 44 (4) (2009) 263–271. doi:10.1243/03093247JSA478.
- [24] C. E. Hunt, E. M. Schulson, Recrystallization of zircaloy-4 during transient heating, *Journal of Nuclear Materials* 92 (2-3) (1980) 184–190. doi:10.1016/0022-3115(80)90101-4.
- [25] A. Chaieb, Comportement anisotherme et rupture des gaines combustibles en alliages de zirconium. Application à la situation d'accident d'insertion de réactivité (RIA), Ph.D. thesis, Université Paris-Sciences-et-Lettres (2019).
- [26] G. Trégo, Comportement en fluage à haute température dans le domaine biphasé ($\alpha + \beta$) de l'alliage M5., Ph.D. thesis, Ecole Nationale Supérieure des Mines de Paris (2011).
- [27] J. E. Romero Ospina, Texture Evolution During Beta-quenching of a Zirconium Alloy, Ph.D. thesis, University of Manchester (2010).